The Journal of Green Energy and Environmental Engineering

Research Paper

Degradation Process and Mechanism of Dissolved Organic Matter in Microplastics under Ultraviolet Light

Apostolos Barouta[1], Jorge Orosa[2,*]

[1] Department of Environmental Engineering, Technical University of Denmark, DK-2800 Kongens Lyngby, Denmark
[2] Universidade daCoruña, Campus Industrial de Ferrol, CITENI-Grupo de Polímeros, C/Dr Vazquez Cabrera s/n, Ferrol, Spain
*Corresponding author: Jorg.Orosa@gmail.com

Abstract. Microplastic dissolved organic matter not only endangers human health, causes damage to the immune barrier and affects agricultural production, but also interacts with environmental components such as heavy metals and antibiotics, exacerbating environmental pollution. In this study, the degradation process and transformation mechanism of five microplastic dissolved organic matter (MPDOM) under ultraviolet irradiation were studied by ultraviolet-visible spectrophotometry, three-dimensional fluorescence combined with parallel factor analysis, Fourier transform infrared spectroscopy and Fourier transform ion cyclotron resonance mass spectrometry. The results showed that PSDOM and PETDOM had the best degradation effect under UV irradiation, and the degradation effect of PPDOM was poor. The analysis of UV spectra and three-dimensional fluorescence spectra showed that PSDOM and PETDOM had a high degree of aromaticity and humification, and contained more unsaturated aromatic structures (benzene ring, conjugated double bond, etc.) and fluorescent components (humus, etc.). The above structures and components were preferentially degraded under ultraviolet light. In addition, the mass difference network analysis of MPDOM before and after degradation was carried out to explore the main transformation pathways involved in the degradation process. The results showed that the five MPDOM all underwent a series of reactions (oxygen addition reaction, decarboxylation reaction and dealkylation reaction, etc.) dominated by oxygen addition (+O, +O2, and +O3, etc.) to degrade unsaturated aromatic structures and humus into small molecules under UV irradiation. In addition, the precursor compounds of PPDOM also contain some sulfur-containing compounds, which are mainly degraded by desulfonation reaction. This study reveals the degradation characteristics and molecular transformation mechanism of five microplastics dissolved organic matter under ultraviolet light irradiation, which is helpful to further understand the harm of microplastics dissolved organic matter and its degradation products to the environment.

Keywords: *Microplastic dissolved organic matter (MPDOM); Light degradation; Spectral analysis; Fourier transform infrared spectrum; Mass disparity network analysis*

Received on 15 Feb 2025, Accepted on 15 April 2025, Published on 15 May 2025

1 Introduction

The pervasive environmental contamination by microplastics, synthetic polymer particles ubiquitously fragmented from macroscopic waste, represents a critical challenge of the Anthropocene. While significant research has delineated their global sources, distribution pathways, and ecological interactions, a profound and growing concern lies in the soluble fraction they release: microplastic-derived dissolved organic matter (MPDOM). As microplastics undergo environmental aging through physical weathering, chemical oxidation, and biological activity, they leach a complex cocktail of organic compounds into the surrounding water, forming MPDOM [4]. This constitutes a novel and mobile pool of dissolved carbon, distinct from natural dissolved organic matter (NDOM) in its origin and molecular signature, yet capable of participating in similar biogeochemical processes. The environmental implications of MPDOM are severe and multifaceted. It not only introduces direct toxicity, with components like phthalates linked to endocrine disruption and immune system damage in organisms [12], but also acts as a dynamic vector in contamination scenarios. MPDOM can complex with heavy metals, adsorb onto minerals, and interact with pervasive pollutants like antibiotics, thereby altering the mobility,

bioavailability, and combined toxic effects of these contaminants [6, 7]. In agricultural contexts, its intrusion disrupts essential soil nutrient cycles and negatively impacts crop health by impairing root-associated enzyme activities, threatening food security [8-11]. Consequently, MPDOM transitions the microplastic problem from a particulate issue to a more dissolved and bioavailable chemical threat, exacerbating environmental pollution and posing risks to ecosystem integrity and human health [13]. Understanding the environmental fate and transformation pathways of MPDOM is therefore paramount for a complete assessment of plastic pollution's impact.

A dominant and inevitable transformation pathway for MPDOM in sunlit surface waters is photodegradation driven by ultraviolet (UV) radiation. This process is initiated by chromophoric and auxochromic groups within the MPDOM molecules. Similar to NDOM, structures such as aromatic rings and conjugated double bonds absorb UV photons, leading to the formation of excited-state species and highly reactive oxygen species (ROS) like hydroxyl radicals (•OH), singlet oxygen ($^1O_2$), and triplet-state DOM (^{3}DOM*) [14, 39]. These ROS, in turn, attack and mineralize or structurally alter the MPDOM molecules themselves [15]. Crucially, the efficiency and mechanistic pathway of this photodegradation are intrinsically dictated by the chemical architecture of the parent polymer from which the MPDOM is leached. As highlighted by Zhang et al. [16], MPDOM rich in unsaturated aromatic structures, such as that derived from polystyrene (PS) or polyethylene terephthalate (PET), is predominantly degraded via •OH radical attack on the aromatic cores. In contrast, MPDOM from more aliphatic polymers like polylactic acid (PLA) or polypropylene (PP) undergoes oxidation mainly through $^1O_2$ targeting aliphatic side chains, with unsaturated aromatic molecules generally exhibiting greater photoreactivity. This establishes a clear structure-activity relationship where the inherent polymer identity dictates the environmental persistence and degradation trajectory of its soluble leachates [16-18]. However, significant knowledge gaps persist. While studies have begun to acknowledge MPDOM's role, systematic comparative analyses of the photodegradation kinetics and molecular-scale transformation mechanisms for MPDOM from a spectrum of structurally diverse common polymers remain scarce. The specific fluorescent components (e.g., humic-like vs. protein-like substances) that are preferentially degraded, and the dominant reaction networks (e.g., oxygenation, decarboxylation, dealkylation) that govern the breakdown, are poorly resolved at the molecular formula level. A deep mechanistic understanding is essential to predict the long-term environmental fate of MPDOM and the chemical nature of its degradation products, which may possess their own ecological risks.

To address these critical gaps, this study presents a comprehensive, multi-method investigation into the photodegradation processes and molecular transformation mechanisms of MPDOM derived from five prevalent microplastics with distinct structural backbones: PS, PET, poly(butylene adipate-co-terephthalate) (PBAT), PLA, and PP. We aim to first quantify and compare their macroscopic photodegradation efficiencies under simulated UV irradiation. Subsequently, we employ a suite of advanced spectroscopic and mass spectrometric techniques to unravel the degradation process at increasing levels of detail: from tracking bulk chromophore loss via UV-Vis spectrophotometry, to identifying and quantifying the degradation of specific fluorescent components using three-dimensional excitation-emission matrix (3D-EEM) spectroscopy coupled with parallel factor analysis (PARAFAC), and finally to achieving unprecedented molecular-level insights via Fourier transform ion cyclotron resonance mass spectrometry (FT-ICR-MS). The FT-ICR-MS analysis, complemented by Van Krevelen diagrams and mass difference network analysis, allows us to move beyond bulk properties to identify molecular formulas, calculate aromaticity indices, categorize compound classes, and, most importantly, map the precise chemical transformations (e.g., +O, +H_2O_2, -CO_2, -CH_2) that connect precursor and product molecules during photolysis. By integrating data from these complementary techniques, this research systematically links the initial polymer structure to the composition and photoreactivity of its corresponding MPDOM, and ultimately elucidates the specific reaction pathways that underpin its environmental degradation. The findings are expected to provide a fundamental mechanistic framework essential for accurate environmental risk assessment of plastic pollution and to inform future mitigation strategies.

In view of this, this study selected lignosulfonate sodium as the raw material, chitosan as the functional modifier, and polyvinyl alcohol as the network crosslinking film-forming promoter. Using a multiple cross-linking induction strategy, a lignin-based liquid mulch film (LCP) with excellent mechanical and water vapor barrier properties was prepared. Physicochemical structure characterization was used to systematically explore the intermolecular interaction mechanisms in the synthesis of the ternary composite liquid mulch film of lignosulfonate sodium/chitosan/polyvinyl alcohol. The responsiveness between its rheological properties, mechanical strength,

water vapor barrier performance, and crop growth and soil retention characteristics was studied. The aim is to provide theoretical basis and technical support for the high-value utilization of lignosulfonate and the green transformation of agriculture in arid and semi-arid regions, and it has important practical significance for promoting mulch film reduction, substitution, and sustainable development.

2 Materials and Methods

2.1 Experimental Design

2.1.1 Preparation of MPDOM Stock Solution

Take 5g each of the five microplastics (PS, PET, PBAT, PLA, and PP) and add them to a 1L sterilized beaker, mix with 1L of deionized water, and place in an aging chamber equipped with six 18W UV lamps. Oscillate at 150 $r \cdot min^{-1}$ for 7 days, with the light source wavelength of the UV aging chamber set to 254 nm. During the aging period, periodically add deionized water to the beaker to avoid concentration effects due to water evaporation. Finally, filter the leachates of the five microplastics through a 0.45 μm cellulose acetate membrane to obtain the corresponding supernatant, i.e., the MPDOM stock solution.

2.1.2 Degradation Experiment of MPDOM

Dilute the stock solutions of the five MPDOMs to 10 $mg \cdot L^{-1}$ solutions. Take 20 mL each of the diluted MPDOM solutions and add them to quartz tubes. Degrade under UV irradiation for 12 hours. Compared to the UV aging chamber, the UV light source at this stage is a 300W mercury lamp, with the main emission wavelength concentrated at 365 nm, which better simulates the UV intensity of sunlight reaching the ground. Sampling is performed at 7 time points: 0, 2, 4, 6, 8, 10, and 12 hours, retaining the MPDOM solutions at different degradation times for subsequent measurement and characterization.

2.1.3 Measurement Methods

The TOC concentration of MPDOM was quantitatively measured by a total organic carbon analyzer (Multi N/C 3000). The spectra of MPDOM in the wavelength range of 200~800 nm were measured by an ultraviolet-visible spectrophotometer (TU-1810, bjpersee, Chinese). The three-dimensional fluorescence spectra (EEM) and parallel factor analysis of MPDOM were determined by a fluorescence spectrophotometer (F-4600, HITACHI, Japan). The infrared spectra of MPDOM powder in the wavelength range of 600~4000 cm^{-1} were measured by a Fourier transform infrared spectrometer (ATR-FTIR, Perkinelmer, USA). The relative molecular weight of MPDOM was determined by high-performance liquid chromatography (Thermo-U3000). The MPDOM solution was concentrated by solid-phase extraction, and then the molecular composition of the samples was determined using a Fourier transform ion cyclotron resonance mass spectrometer in negative ion mode with an ESI source. The collected mass-to-charge ratio range was 100~1600.

2.2 Analytical Methods

2.2.1 Spectral Data Analysis

Studies have shown that in the UV spectra of MPDOM, the UV absorption coefficient at 254 nm (a254) is proportional to the relative concentration of DOM. Therefore, this study selected a254 to characterize the changes in relative concentration of the five MPDOMs during the degradation process [19,20]. DOM contains many fluorescent substances that exhibit fluorescence at different wavelengths under UV irradiation. According to literature reports, three-dimensional fluorescence spectra can be divided into five regions [21]: aromatic protein regions (Regions I, II: Ex 200-250 nm, Em 280-350 nm), fulvic acid region (Region III: Ex 200-250 nm, Em 400-450 nm), microbial byproduct region (Region IV: Ex 250-300 nm, Em 300-380 nm), and humic acid region (Region V: Ex 250-400 nm, Em 400-550 nm). The components and content of MPDOM can be determined based on the fluorescence intensity of each component in its fluorescence spectrum. Since the humification index (HIX) is proportional to polycyclic aromatic hydrocarbon content and inversely proportional to the percentage of oxygen-containing functional groups and the mineralization rate of DOM [22], this study selected the HIX index to represent the humification level and aromaticity of MPDOM. Furthermore, as the three-dimensional fluorescence data of MPDOM are relatively complex, this study used parallel factor analysis to divide it into

different components [23]. It mainly includes three components: C1, C2, and C3. The Ex and Em wavelengths of component C1 are 252 nm and 302 nm, respectively, belonging to protein-like substances. The Ex and Em wavelengths of components C2 and C3 are 236 nm, 246 nm and 408 nm, 246 nm, respectively, both belonging to humic-like substances. Among them, component C3 has a longer emission wavelength and is associated with terrestrial humic-like components [24].

2.2.2 Molecular Characteristic Analysis

This study performed screening, classification, calculation of relative molecular mass, and other analytical processes on the raw FT-ICR-MS data [25]. The modified aromaticity index (AImod) was selected to describe molecular aromaticity, where the value of AImod is proportional to the aromaticity of the compound [26]. Furthermore, the Van Krevelen (VK) diagram in this study further subdivided dissolved organic matter into seven categories based on different ranges of O/C and H/C [27]: lipid-like region, aliphatic/protein-like region, carbohydrate-like region, highly unsaturated and phenolic compounds region, lignin/CRAM-like region, tannin-like region, and condensed aromatic region. Each point in the VK diagram represents one or a series of DOM molecules with specific H/C and O/C ratios [28].

2.2.3 Mass Difference Network Analysis

According to existing reports, the main reaction types involved in the degradation process of MPDOM include four categories: oxidation, decarboxylation, reduction, and dehydration [29]. Molecular substances in the degradation process can be divided into three types: precursors, products, and recalcitrant components. Using Gephi software for visualization processing, mass difference network analysis was conducted to identify precursor-product pairs in the reaction process, thereby analyzing potential reaction pathways. In the molecular network diagram, nodes represent the molecular formulas of compounds in DOM, and the connections between nodes are defined as edges, representing the transformation pathways between these compounds [30]. By analyzing the reaction pathways of MPDOM during degradation and further combining them with analytical methods such as UV spectroscopy and fluorescence spectroscopy, the intrinsic molecular transformation mechanism was explored.

2.3 Data Processing

This study used Origin 2021 software to plot UV spectra and infrared spectra. For the raw data of three-dimensional fluorescence spectra, first-order and second-order Rayleigh and Raman scattering were removed, and Raman normalization was performed using blank water samples [31]. According to the method proposed by Li et al. [32], the processed data was imported into MATLAB R2021b software via the DOMFluor toolbox for further processing and analysis. After exporting the data, Origin 2021 software was used for plotting. During the parallel factor analysis, the data needs to be uploaded to the openfluor database to screen for data groups with component similarity above 95%. After successfully confirming that the three-component model passed the split-half test, residual analysis and loading analysis were performed [33,34]. For the raw data from Fourier transform ion cyclotron resonance mass spectrometry (FT-ICR-MS), after preprocessing, indicators such as the modified aromaticity index (AImod) and aromaticity equivalent (Xc) were calculated [35-37]. Then, Gephi software and Origin software were used to visualize the mass differences of precursors and products of MPDOM during the degradation process.

3 Results and Discussion

3.1 Analysis of TOC Degradation Effect and Transformation Mechanism

The absorbance of the five MPDOMs in the range of 200~600 nm and the DOC concentration degradation rates before and after 12 hours are shown in Fig. 1. Overall, absorbance decreased with increasing wavelength, and the main UV absorption peaks formed in the range of 200~400 nm. Before irradiation, PSDOM and PETDOM had higher absorbance in the 200~300 nm range, with relatively obvious absorption peaks in the 240~290 nm range. According to Zhou et al. [38], this indicates that PSDOM and PETDOM contain a certain number of aromatic structures and conjugated double bonds, etc. After irradiation, as degradation time accumulated, the absorbance of all five MPDOMs also continuously decreased, indicating that UV irradiation had a degradation effect on all

types of MPDOM. However, overall, the decrease in absorbance was most significant for PSDOM and PETDOM (Fig. 2), and their TOC degradation effects were the best, with degradation rates of 35.8% and 28.0%, respectively. In contrast, the degradation effects of PBATDOM, PLADOM, and PPDOM were poorer, with TOC degradation rates of 14.9%, 18.0%, and 12.7%, respectively. This may be because PSDOM and PETDOM contain more unsaturated aromatic structures. Unsaturated aromatic molecules have stronger light absorption capacity and are more easily degraded, thus manifesting as a significant decrease in absorbance in the UV spectra.

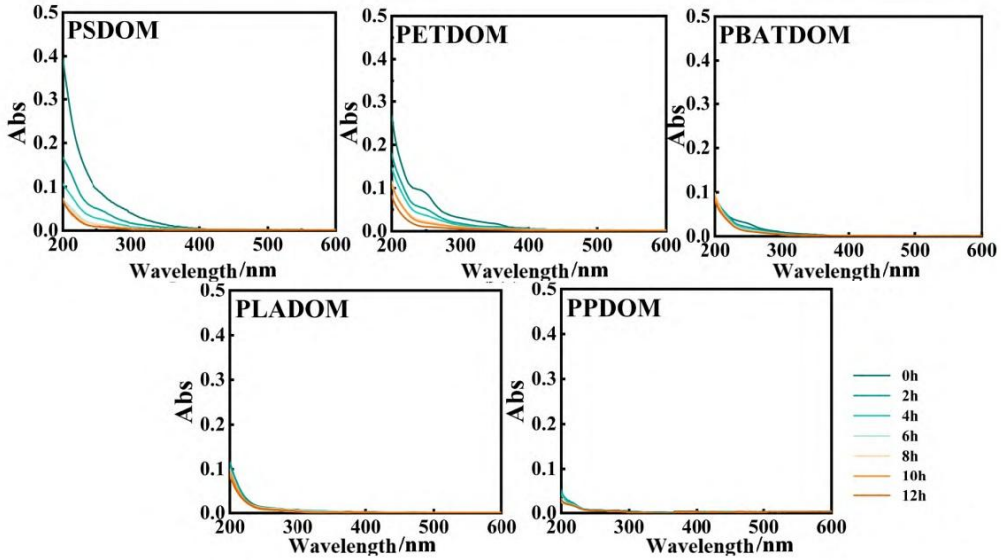

Figure 1 Ultraviolet-vis spectra

The UV absorption coefficient at 254 nm (a254) of MPDOM is proportional to the relative concentration of DOM. This study compared and analyzed the changes in a254 of the five MPDOMs over degradation time. As shown in Fig. 1, within 0~12 hours, the a254 of PSDOM, PETDOM, and PBATDOM showed a downward trend, with the former two decreasing rapidly and PBATDOM decreasing slowly. In contrast, the a254 of PLADOM and PPDOM at 254 nm showed basically no change before and after UV irradiation. Guo et al. [39] mentioned in their research that after absorbing light, DOM produces singlet DOM (^{1}DOM), which can further form triplet DOM (^{3}DOM). ^{3}DOM* can not only directly interact with pollutants but also further produce •OH and $^1O_2$, etc., affecting the photochemical behavior of organic pollutants in water.

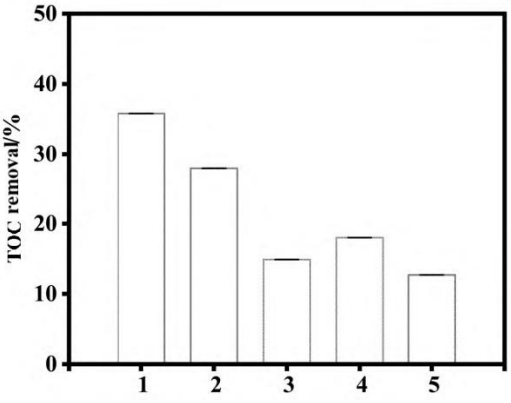

Figure 2 Degradation rate of TOC

Simultaneously, MPDOM also reacts with free radicals in water, destroying structures such as conjugated dienes and benzene rings, leading to changes in its own structure and properties. Wang et al. [40] mentioned in their research that indirect photolysis plays a more important role in the photodegradation of DOM, which includes oxidation-reduction reactions with ROS such as ^{3}DOM*, •OH, and $^1O_2$ produced by MPDOM absorbing light. Due

to containing more unsaturated aromatic structures and conjugated double bonds, etc., PSDOM and PETDOM were destroyed by •OH and $^1O_2$ during degradation, resulting in a significant decrease in absorbance before and after degradation.

3.2 Three-Dimensional Fluorescence Analysis

3.2.1 Fluorescence Spectra Analysis

As can be seen from Fig. 3, the initial fluorescence peak intensities of the three MPDOMs containing benzene rings, PSDOM, PETDOM, and PBATDOM, were all higher than those of the other two MPDOMs. The fluorescence peaks of PSDOM, PETDOM, and PBATDOM were mainly distributed in the humic acid and fulvic acid regions, also containing a small amount of aromatic protein. Studies have shown that the fluorescence signals of MPDOM in the humic acid region correspond to compounds such as aromatic ketones [41]. The fluorescence peaks of PLADOM and PPDOM were mainly distributed in the aromatic protein region. After 12 hours of degradation under mercury lamp irradiation, the DOC-normalized fluorescence intensity significantly decreased across wavelengths, indicating the photochemical sensitivity of fluorophores to UV irradiation. Among them, the fluorescence peak intensity of PLADOM showed basically no change. Compared to before irradiation, a new fluorescence peak appeared in the microbial byproduct region for PPDOM. For PSDOM, PETDOM, and PBATDOM, the fluorescence maps mainly showed aromatic protein and fulvic acid signals, and the fluorescence intensity in the humic acid region almost disappeared, indicating that humic-like substances were preferentially degraded by ultraviolet light. Based on this, this study calculated the HIX values of the five MPDOMs to analyze their humification level and aromaticity. The results are shown in Table 1. The initial HIX values of PSDOM, PETDOM, and PBATDOM were higher, all greater than 6, indicating a higher degree of humification and aromaticity for these three MPDOMs [42]. After 12 hours of degradation, the HIX value of PPDOM showed basically no change, while the HIX values of the other four MPDOMs decreased significantly. Since the HIX index is proportional to polycyclic aromatic hydrocarbon content, and polycyclic aromatic hydrocarbons are typical conjugated systems, this is consistent with the UV spectra in Fig. 1. These results indicate that the higher degradation efficiency of PSDOM and PETDOM can be attributed to their containing more conjugated systems and humic acid-like substances.

Table 1 HIX values of five microplastics before and after irradiation

Item	PSDOM	PETDOM	PBATDOM	PLADOM	PPDOM
Before irradiation	0.79	0.89	0.89	0.28	0.25
After irradiation	0.29	0.25	0.41	0.17	0.26

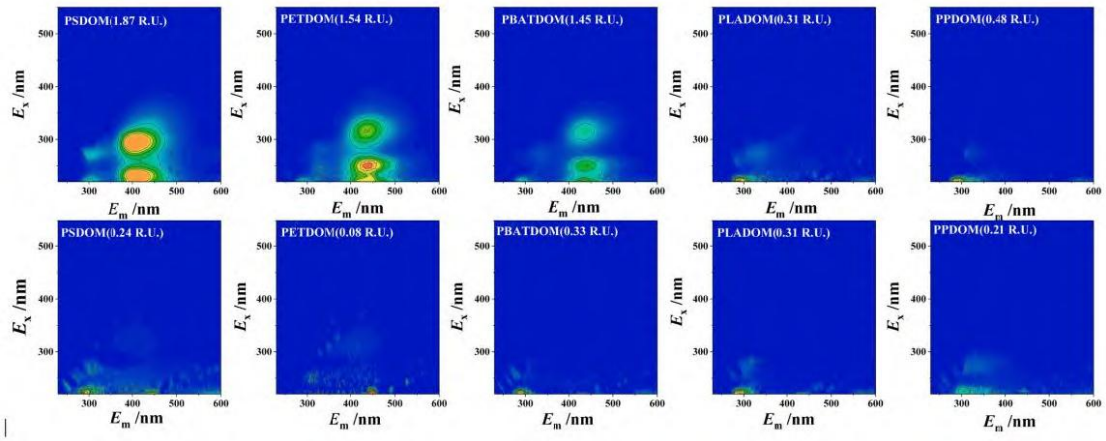

Figure 3 Three-dimensional fluorescence spectra before and after UV irradiation

3.2.2 Parallel Factor Analysis

As shown in Fig. 4, after parallel factor analysis, all five MPDOMs contained the following three components: C1 (aromatic protein-like), C2 (humic-like), and C3 (terrestrial humic-like) [43]. Figure 5 shows the change trends of

the fluorescence intensity (Fmax) of the three components of MPDOM with degradation time. The Fmax degradation rates of the three components of PSDOM and PETDOM after 12 hours of UV irradiation were basically above 90%. In contrast, the C3 component of PBATDOM did not show a significant decrease. The Fmax of all three components of PLADOM did not decrease significantly. The Fmax of the C1 component of PPDOM did not decrease significantly, which is consistent with the fluorescence spectra of MPDOM before and after degradation. Overall, UV light caused the most obvious damage to PSDOM and PETDOM. Combined with the UV spectra and TOC degradation efficiency mentioned above, it basically indicates that PSDOM and PETDOM contain more unsaturated aromatic structures and conjugated double bonds, etc. Such structures are preferentially degraded during UV irradiation, so the TOC degradation rates of PSDOM and PETDOM are higher compared to other MPDOMs.

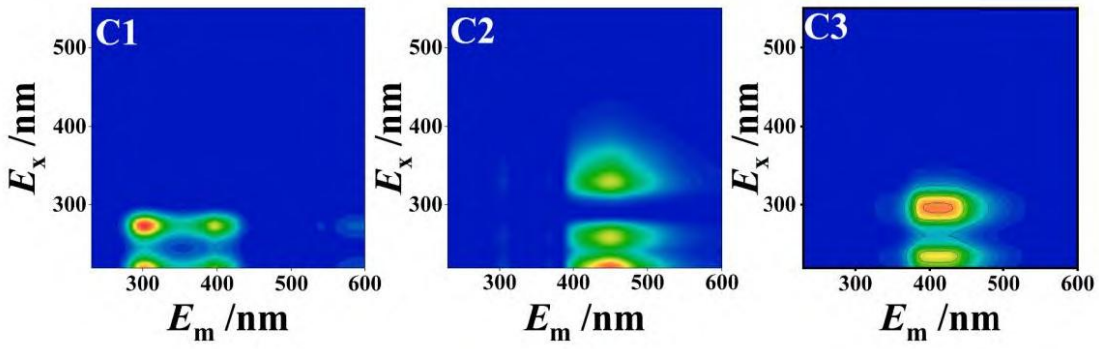

Figure 4 PARAFAC model output showing three different fluorescent components

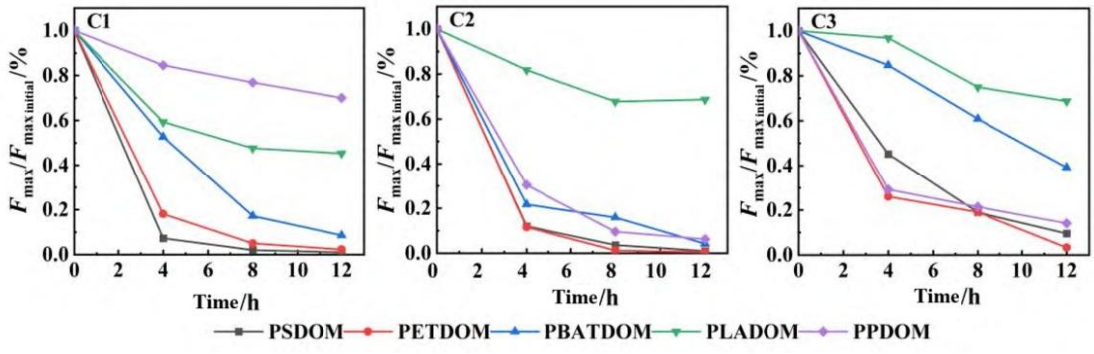

Figure 5 Changes of Fmax / Fmax initial of three fluorescent components after photolysis

3.3 Molecular Characteristic Analysis

The FT-ICR-MS determination results of the five MPDOMs are shown in Fig. 6. Before irradiation, the numbers of molecular formulas for MPDOM were 3075, 2270, 2128, 736, and 1429, respectively. The molecular numbers of PSDOM, PETDOM, and PBATDOM were much larger than those of the latter two. Since these three microplastics all contain benzene rings, it indicates that MPDOM derived from benzene ring-containing polymers may have more complex molecular structures. After irradiation, the number of molecular formulas for PSDOM and PETDOM decreased significantly, which is consistent with the results of UV spectroscopy, indicating that most of the unsaturated aromatic structures contained in PSDOM and PETDOM were degraded. The number of molecular formulas for PLADOM increased. This may be because the large molecules generated in the early stage of UV degradation of PLADOM were degraded, producing more small molecular compounds, leading to an increase in its number of molecular formulas. In contrast, although the number of molecular formulas for PBATDOM and PPDOM decreased, it was not significant, which is consistent with the characterization of insignificant decrease in UV absorbance during degradation. The aromaticity index (AImod) and aromaticity equivalent (Xc) are two indicators commonly used to represent the aromaticity of MPDOM. A higher AImod value indicates stronger aromaticity of MPDOM, and a larger Xc value indicates a greater number of aromatic rings contained [44]. As can be seen from Fig. 6, the AImod values of PSDOM and PETDOM were 0.41 and 0.39,

respectively, much higher than those of the other three MPDOMs, indicating that PSDOM and PETDOM have the highest aromaticity. At the same time, the Xc values of these two MPDOMs are also high, indicating that they contain more aromatic rings. Furthermore, studies have shown that based on the calculation results of the Xcwa value (weighted index), it can be determined whether MPDOM contains condensed aromatic units [45]. The Xcwa values for PSDOM and PETDOM were 2.7824 and 2.7819, respectively, both greater than 2.7143, indicating that PSDOM and PETDOM have a high degree of condensed aromaticity. In contrast, PBATDOM, which also contains benzene rings, had an Xcwa of 2.6216, less than 2.7143, meaning it did not exhibit condensed aromaticity at the molecular level. This may be because microplastic PBAT is biodegradable, and the benzene rings in its derivative PBATDOM are more easily broken under UV irradiation.

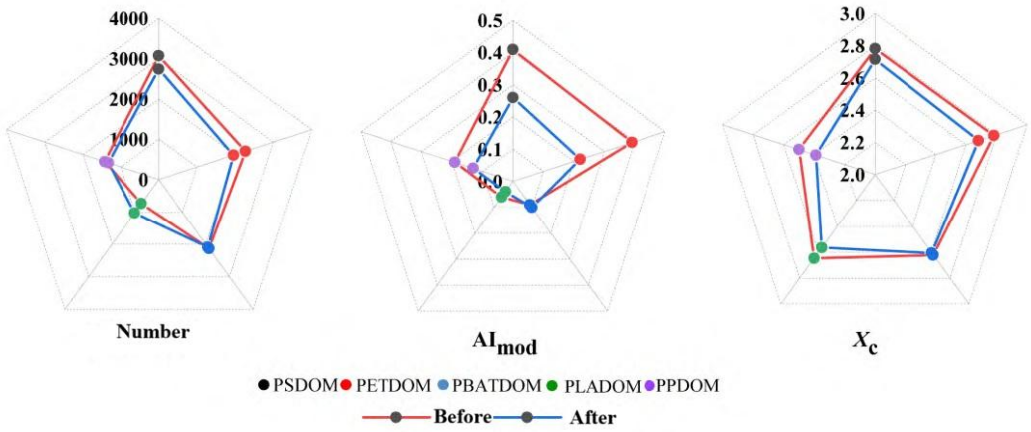

Figure 6 Changes in number of molecule formulas, AImod values, and Xc values of five types of MPDOM before and after irradiation

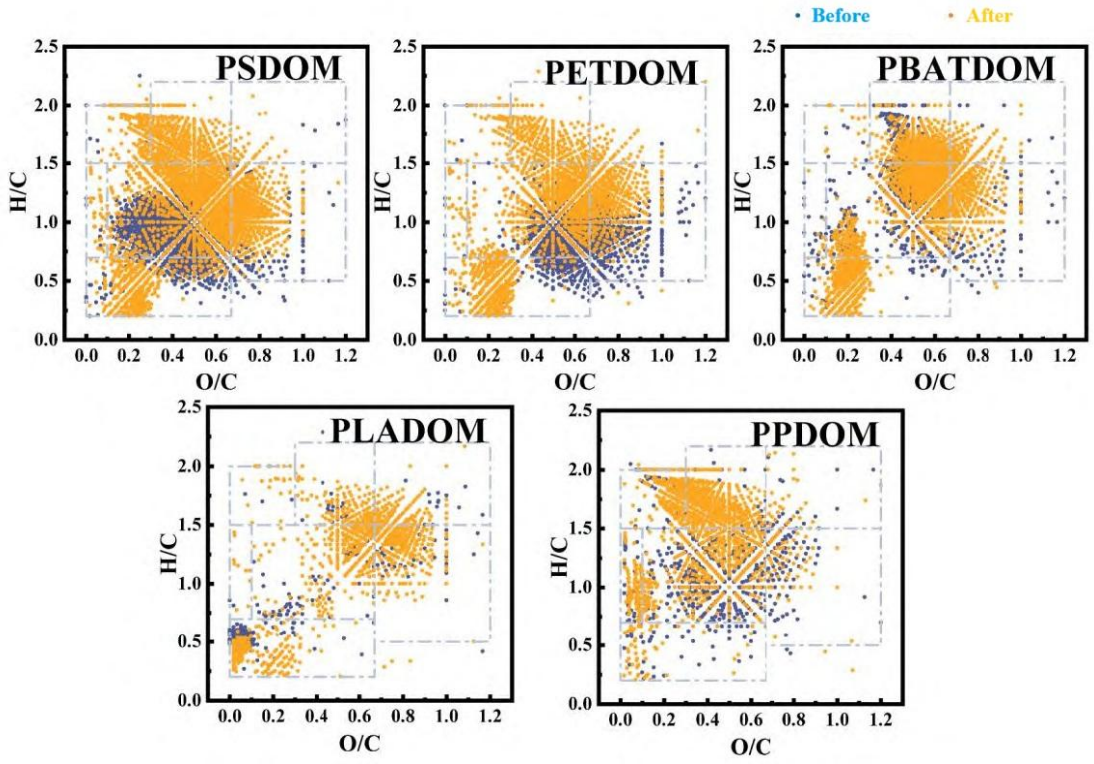

Figure 7 The van Krevelen (VK) diagram of five MPDOM before and after degradation

Figure 7 shows the VK diagrams of the five MPDOMs. Before irradiation, the molecules of PSDOM and PETDOM

were mainly distributed in the lignin/CRAM-like region, i.e., the region with lower H/C. The other three MPDOMs were mainly distributed in the high H/C region. PBATDOM molecules were mainly distributed in the carbohydrate-like, lignin/CRAM-like, and tannin-like regions. PLADOM molecules were mainly distributed in the aliphatic/protein-like, carbohydrate-like, tannin-like, and condensed aromatic regions. PPDOM was distributed more evenly, with a large number distributed in the lipid-like, aliphatic/protein-like, highly unsaturated and phenolic, and lignin/CRAM-like regions. After irradiation, the proportion of PSDOM and PETDOM molecules in the lignin/CRAM-like region decreased, and the proportional number in the lipid-like, aliphatic/protein-like, highly unsaturated and phenolic, and condensed aromatic regions increased. The molecular distribution of PBATDOM, PLADOM, and PPDOM showed little difference from before UV irradiation. Studies have shown that the lignin/CRAM-like component can promote the generation of reactive oxygen species (^{3}DOM*, •OH, and $^1O_2$, etc.), thereby further promoting MPDOM degradation. Therefore, for PSDOM and PETDOM, which contain more lignin-like molecules, they may exhibit better degradation effects during irradiation.

3.4 Mass Difference Network Analysis

As shown in Fig. 8, the reaction types involved by MPDOM in this study mainly include dealkylation, oxygenation, decarboxylation, deamination, nitroso compound reactions, and desulfonation. As shown in Fig. 9, the reactions undergone by the five MPDOMs under UV irradiation were all dominated by oxygenation reactions, also involving dealkylation, decarboxylation, and nitroso compound reactions. The reaction types for PPDOM additionally involved deamination and desulfonation reactions. In the reaction process of PSDOM, a total of 1053 reactions were involved, of which 407 were oxygenation reactions, accounting for 38.7%. Combined with Fig. 8, it can be seen that the main oxygenation reactions involved were $+H_2O_2$ (133), $+O_3$ (116), $+O_2$ (57), and +O (37). From Fig. 10, it can be seen that the two main precursor compounds of PSDOM, $C_{15}H_{21}O_{11}$ and $C_{18}H_{25}O_{13}$, generated $C_{15}H_9O_{12}$ and $C_{18}H_{23}O_{14}$ through oxygenation reactions.

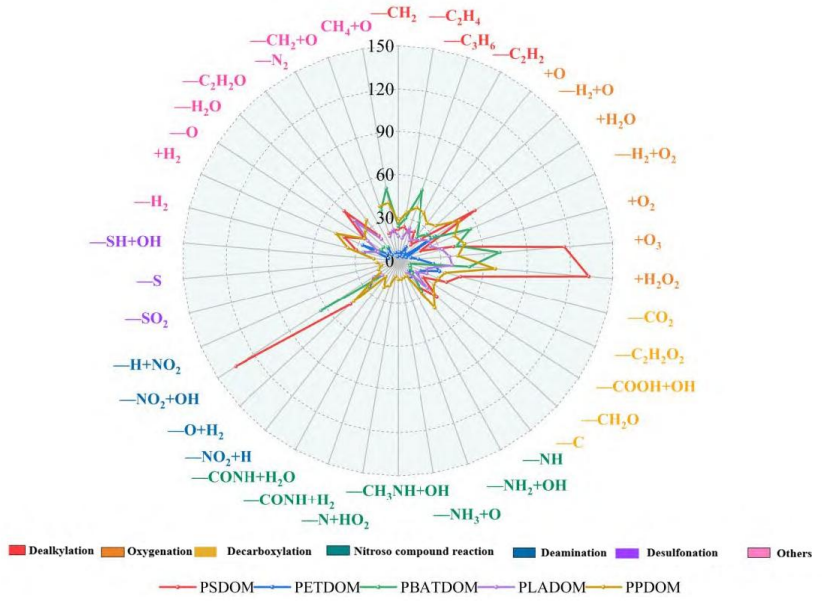

Figure 8 Reaction pathways of the five MPDOM and their quantities

PETDOM underwent 326 reactions, involving 96 oxygenation reactions, accounting for 29.4%, mainly including $+H_2O_2$ (25), $+O_3$ (14), $+O_2$ (15), and +O (11), etc. Its main precursor compounds, $C_{21}H_{17}O_{11}$ and $C_{20}H_{17}O_9$, generated molecules such as $C_{26}H_5O_4$ and $C_{25}H_5O_4$ through decarboxylation reactions. PBATDOM underwent a total of 747 reactions, involving 295 oxygenation reactions, accounting for 39.5%. Specific reaction pathways included $+O_2$ (97), $+O_3$ (71), $+H_2O_2$ (50), and +O (48), etc. Its main precursor compounds were $C_{33}H_{21}O_5$ and $C_{29}H_{25}O_5$, which generated molecules such as $C_{33}H_{19}O_7$ and $C_{29}H_{27}O_6$ through oxygenation reactions. PLADOM underwent a total of 565 reactions, involving 197 oxygenation reactions, accounting for 34.9%, mainly including $+O_2$ (57), +O (40), $+H_2O_2$ (38), and $+O_3$ (36), etc. Its main precursor compounds, $C_{54}H_{29}O$ and $C_{52}H_{25}O_2$, generated many small molecules such as $C_{29}H_{39}O_{20}$ and $C_{27}H_{37}O_{21}$ through oxygenation reactions. Compared to other MPDOMs, the

precursor compounds of PPDOM contained some sulfur compounds. Therefore, besides oxygenation and decarboxylation reactions, etc., desulfonation reactions also occurred: The precursor compound $C_{28}H_{29}O_2$ of PPDOM generated $C_{28}H_{27}O_4$ through $+O_2$, and $C_{27}H_{29}OS$ generated $C_{22}H_{39}O_8$ through -SH.

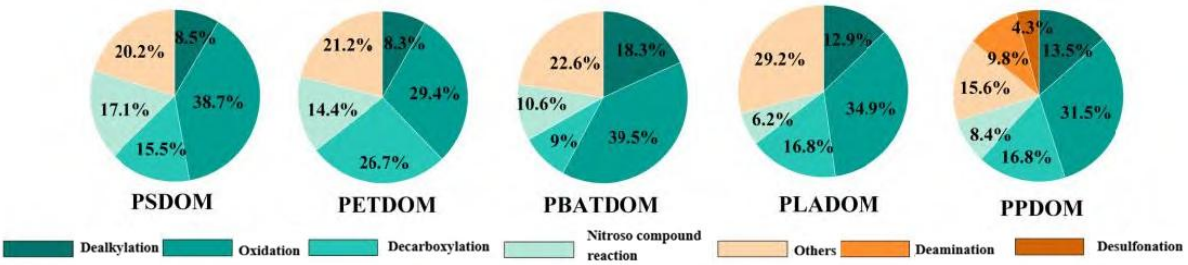

Figure 9 Seven reaction types of five MPDOM and their proportions

Based on the comprehensive experimental findings presented in this study, a deeper discussion on the degradation disparities and underlying molecular mechanisms of MPDOM from different polymers is warranted. The pronounced variability in photodegradation efficiency, with PSDOM and PETDOM showing superior degradation (35.8% and 28.0% TOC removal) compared to the aliphatic PLADOM and PPDOM (18.0% and 12.7%), is fundamentally rooted in their distinct molecular architectures. The analytical data collectively paints a coherent picture: PSDOM and PETDOM initially exhibit higher UV absorbance, particularly in the 240-290 nm range, and possess significantly greater HIX values (0.79 and 0.89) and modified aromaticity indices (AImod of 0.41 and 0.39). This confirms their enrichment in unsaturated aromatic structures, such as benzene rings and conjugated systems, which are potent chromophores. These structures are inherently more photoreactive because they efficiently absorb UV photons, leading to the formation of excited triplet states (^{3}DOM*) and subsequently, reactive oxygen species (ROS) like hydroxyl radicals (•OH) and singlet oxygen ($^1O_2$). The generated ROS then attack and fragment these very aromatic cores, leading to effective degradation. This is further corroborated by the parallel factor analysis, which showed the near-complete degradation (>90% reduction in Fmax) of humic-like and protein-like fluorescent components in PSDOM and PETDOM, components often associated with complex aromatic networks. Conversely, the saturated aliphatic backbones of PLADOM and PPDOM lack such efficient light-harvesting chromophores, resulting in lower ROS yields and a slower, less efficient degradation process primarily targeting side chains. The Van Krevelen diagram analysis provides crucial spatial context: the pre-irradiation molecules of PSDOM and PETDOM were predominantly clustered in the lignin/CRAM-like region (low H/C), a category known for its photoreactivity and propensity to generate ROS. Their degradation shifted the molecular population towards regions with higher H/C ratios, visually mapping the breakup of complex, aromatic cores into smaller, more aliphatic fragments. The case of PBATDOM presents an interesting intermediate; while containing aromatic rings from its terephthalate units, it demonstrated lower condensed aromaticity (Xcwa < 2.7143) and moderate degradation, possibly due to the biodegradable nature of its aliphatic ester segments influencing overall stability. Furthermore, the unique behavior of PPDOM, which involved desulfonation reactions, highlights how polymer-specific additives or manufacturing byproducts (sulfur-containing compounds) can dictate unique degradation pathways, adding another layer of complexity to MPDOM's environmental transformation.

The environmental implications of these findings are profound and extend beyond a mere ranking of polymer degradability. This study elucidates that the threat of microplastics is dynamically compositional; as particles age, they release a cocktail of soluble compounds (MPDOM) whose environmental persistence and transformation are dictated by the parent polymer's "molecular memory." The demonstrated structure-activity relationship means that aromatic polymers like PS and PET, while fragmenting slower than some aliphatic ones, may release a more reactive and readily photodegradable dissolved fraction. This photodegradation, however, is not a simple cleansing process. The mass difference network analysis reveals it to be a complex sequence of molecular transformations—dominated by oxygenation ($+H_2O_2$, $+O_3$, $+O_2$) but also involving decarboxylation and dealkylation—that progressively break down large, aromatic humic-like substances into a spectrum of smaller, more oxidized molecules. The ecological impact of these transformation products remains largely unknown. Some may be

mineralized to CO_2, while others could persist as refractory, potentially bioavailable organic acids or other intermediates with unknown toxicity. The multi-methodological approach employed here, especially the powerful synergy between FT-ICR-MS and mass difference network analysis, provides a template for future research to track these products and assess their risks. For instance, the increase in molecular formula count for PLADOM post-irradiation suggests the production of a diverse suite of small molecules worthy of toxicological scrutiny. From a mitigation perspective, understanding that lignin/CRAM-like MPDOM components are both environmentally significant and photolabile could inform advanced oxidation process design for wastewater treatment targeting plastic leachates. Ultimately, this research underscores that microplastic pollution assessments must evolve to consider the differential leaching and degradation kinetics of the dissolved organic fraction. The long-term environmental impact of a microplastic particle is not only a function of its physical persistence but also of the chemical legacy and evolutionary pathway of the MPDOM it releases, a pathway that is meticulously mapped by the polymer's intrinsic chemical structure and the solar radiation it encounters.

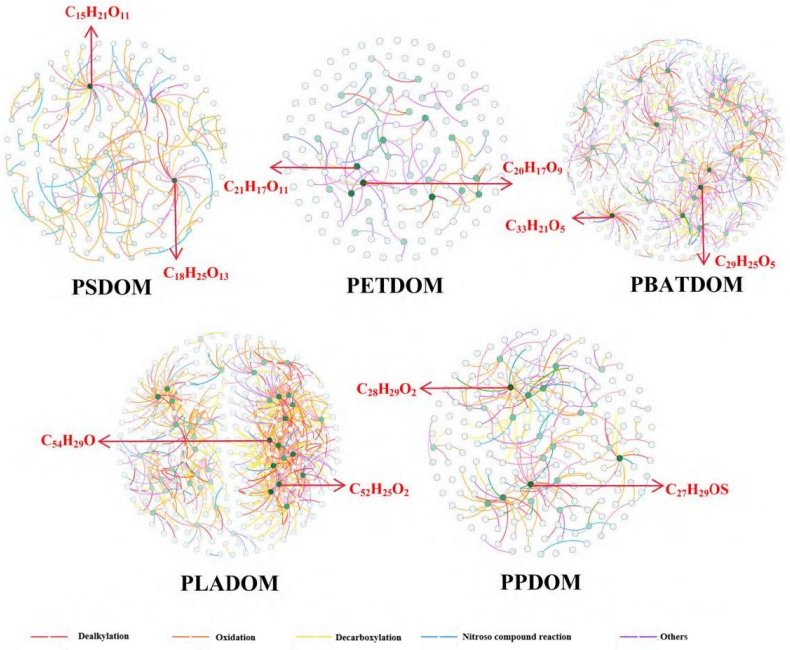

Figure 10 Quality difference network analysis diagrams of five MPDOM

4 Conclusion

By measuring the TOC concentration of MPDOM solutions before and after degradation, it was found that PSDOM and PETDOM had the best degradation effect, while PPDOM had the worst degradation effect. Combined with UV spectroscopy, fluorescence spectroscopy, and parallel factor analysis, it was concluded that PSDOM and PETDOM contain more unsaturated aromatic structures such as benzene rings and phenols, with higher aromaticity and humification degree, and stronger UV absorption capacity. Compared to PLADOM and PPDOM, which have saturated aliphatic structures, they are more easily degraded. The changes in relative molecular mass and molecular characteristics of the five MPDOMs before and after degradation were determined. PSDOM and PETDOM were mainly distributed in the low H/C region and contained more lignin/CRAM-like molecules, which can promote the generation of reactive oxygen species and improve their degradation efficiency. Further mass difference network analysis of MPDOM explored the main reactions occurring during its degradation process. It was summarized that MPDOM mainly completes degradation through a series of oxygenation reactions ($+H_2O_2$, $+O_3$, $+O_2$, and +O, etc.), dealkylation reactions ($-CH_2$, $-C_2H_4$, $-C_3H_6$, and $-C_2H_2$), and decarboxylation reactions ($-CO_2$, $-C_2H_2O_2$, and $-CH_2O$, etc.). Because the precursor compounds of PPDOM contain some sulfur compounds, besides oxygenation and decarboxylation reactions, etc., desulfonation reactions also occurred.

References

[1] Feng X D, Zhang Y N, Jiang Y Q, et al. Spatiotemporal distribution and influencing factors of soil microplastic pollution: A global analysis [J]. Environmental Science, 2026, 47(5), doi: 10.13227/j.hjkx.202504128.

[2] Zhao X W, Li N, Liu T C, et al. Research progress on extraction and detection techniques for microplastics in environmental media and biological samples [J]. Environmental Science, 2026, 47(7), doi: 10.13227/j.hjkx.202505313.

[3] Guo X Y, Ma Y, Cai S Y, et al. Research progress on pollution status and governance of microplastics in the Yellow River Basin [J]. People's Yellow River, 2024, 46(7): 98-111.

[4] Du Z, Li G, Ding S, et al. Effects of UV-based oxidation processes on the degradation of microplastic: Fragmentation, organic matter release, toxicity and disinfection byproduct formation [J]. Water Research, 2023, 237, doi: 10.1016/j.watres.2023.119983.

[5] Gewert B, Plassmann M, Sandblom O, et al. Identification of chain scission products released to water by plastic exposed to ultraviolet light [J]. Environmental Science & Technology Letters, 2018, 5(5): 272-276.

[6] Garba Z N, Zhou W, Lawan I, et al. An overview of chlorophenols as contaminants and their removal from wastewater by adsorption: A review [J]. Journal of Environmental Management, 2019, 241: 59-75.

[7] Liu X F, Zhang L, Du Y Q, et al. Microplastics in China's surface water systems: distribution, driving forces and ecological risk [J]. Journal of Hazardous Materials, 2025, 485, doi: 10.1016/j.jhazmat.2024.136864.

[8] Liu J X, Wang P Y, Wang Y F, et al. Negative effects of poly(butylene adipate-co-terephthalate) microplastics on Arabidopsis and its root-associated microbiome [J]. Journal of Hazardous Materials, 2022, 437, doi: 10.1016/j.jhazmat.2022.129294.

[9] Liu Y Y, Xu F J, Ding L P, et al. Microplastics reduce nitrogen uptake in peanut plants by damaging root cells and impairing soil nitrogen cycling [J]. Journal of Hazardous Materials, 2023, 443, doi: 10.1016/j.jhazmat.2022.130384.

[10] Duan C J, Yang D N, Zhang Z Q, et al. Effects of microplastics on maize growth characteristics and rhizosphere soil enzyme activities [J]. Environmental Science, 2026, 47(8), doi: 10.13227/j.hjkx.202504006.

[11] Zhang Y, Hao S Z, Dou M, et al. Effects of biodegradable microplastics on rhizosphere soil enzyme activities and metabolomics in wheat [J]. Environmental Science, 2026, 47(6), doi: 10.13227/j.hjkx.202504157.

[12] Paluselli A, Fauvelle V, Galgani F, et al. Phthalate release from plastic fragments and degradation in seawater [J]. Environmental Science & Technology, 2019, 53(1): 166-175.

[13] Yang N N, Zuo J E, Zhang Y Y, et al. Research progress on plastic aging process and its environmental hazards [J]. Environmental Science, 2025, 46(3): 1850-1860.

[14] Tang C C, Chen H I, Brimblecombe P, et al. Textural, surface and chemical properties of polyvinyl chloride particles degraded in a simulated environment [J]. Marine Pollution Bulletin, 2018, 133: 392-401.

[15] Tong J, He S Y, Huang X M, et al. The fate, impacts and potential risks of photoaging process of the microplastics in the aqueous environment [J]. Journal of Contaminant Hydrology, 2025, 275, doi: 10.1016/j.jconhyd.2025.104699.

[16] Zhang M W, Ding L, Qiu X R, et al. Interactions between iron minerals and dissolved organic matter derived from microplastics inhibited the ferrihydrite transformation as revealed at the molecular scale [J]. Environmental Science & Technology, 2024, 58, 13478-13489.

[17] Zhang T S, Shang J J, Liu H Y, et al. Characteristics of aging and small particle size particle release of tire microplastics in different environmental media [J]. Environmental Science, 2024, 45(6): 3700-3707.

[18] Liu G Z, Zhu Z L, Yang Y X, et al. Sorption behavior and mechanism of hydrophilic organic chemicals to virgin and aged microplastics in freshwater and seawater [J]. Environmental Pollution, 2019, 246: 26-33.

[19] Zhao Y, Song K S, Lv L L, et al. Relationship changes between CDOM and DOC in the Songhua River affected by highly polluted tributary, northeast China [J]. Environmental Science and Pollution Research, 2018, 25(25): 25371-25382.

[20] D'andrilli J, Silverman V, Buckley S, et al. Inferring ecosystem function from dissolved organic matter optical properties: a critical review [J]. Environmental Science & Technology, 2022, 56(16): 11146-11161.

[21] Lv J J, Dou Y Y, Gong W J, et al. Characterization of dissolved organic matter in hybrid constructed wetlands using three-dimensional excitation-emission matrix fluorescence spectroscopy [J]. Journal of Water Chemistry and Technology, 2019, 41(2): 113-118.

[22] Huang L K, Zhang J Y, Li L L, et al. PM2.5-bound synchronous polycyclic aromatic hydrocarbons and heavy metals in a typical cold city in northern China: Differences in heating and non-heating periods [J]. Journal of Environmental Management, 2025, 381, doi: 10.1016/j.jenvman.2024.125359.

[23] Ding Q W, Wang Z Y, Sun H, et al. Effects and evolution mechanism of UV-AOPs induced aging of microplastics: Fragmentation and organic matter release [J]. Journal of Water Process Engineering, 2025, 75, doi: 10.1016/j.jwpe.2025.108029.
[24] Zhang Z H, Chen X, Li H B, et al. Spectral characteristics of dissolved organic matter in the Yangtze River Basin and its response to natural and anthropogenic activities [J]. Environmental Science, 2025, 46(4): 2135-2144.
[25] Fu Q L, Fujii M, Ma R. Development of a Gaussian-based alignment algorithm for the ultrahigh-resolution mass spectra of dissolved organic matter [J]. Analytical Chemistry, 2023, 95, 2796-2803.
[26] Lin X W, Wu X D, Chen B F, et al. Deciphering the impacts of main inflowing rivers on dissolved organic matter in Lake Daye using isotopes, optical spectroscopy, and FT-ICR MS during non-flood season [J]. Journal of Hydrology, 2025, 663, doi: 10.1016/j.jhydrol.2025.134090.
[27] He Y T, Jarvis P, Huang X, et al. Unraveling the characteristics of dissolved organic matter removed by aluminum species based on FT-ICR MS analysis [J]. Water Research, 2024, 255, doi: 10.1016/j.watres.2024.121429.
[28] Gu Z P, Chen W M, He C, et al. Molecular insights into the transformation of refractory organic matter in landfill leachate nanofiltration concentrates during a flocculation and O_3/H_2O_2 treatment [J]. Journal of Hazardous Materials, 2022, 435, doi: 10.1016/j.jhazmat.2022.128973.
[29] Zhang D R, Luo J W, Li X, et al. Long-term natural photodegradation of plastic films enhances the molecular complexity of plastic-derived dissolved organic matter [J]. Water Research, 2026, 290, doi: 10.1016/j.watres.2025.125139.
[30] Zhong X B, Zhao K Y, Wu M Y, et al. Heavy metals trigger distinct molecular transformations in microplastic- versus natural-derived dissolved organic matter [J]. Environmental Science and Ecotechnology, 2025, 27, doi: 10.1016/j.ese.2025.100610.
[31] Rossi G, Durek J, Ojha S, et al. Fluorescence-based characterisation of selected edible insect species: Excitation emission matrix (EEM) and parallel factor (PARAFAC) analysis [J]. Current Research in Food Science, 2021, 4: 862-872.
[32] Li S D, Hou X, Shi Y, et al. Rapid photodegradation of terrestrial soil dissolved organic matter (DOM) with abundant humic-like substances under simulated ultraviolet radiation [J]. Environmental Monitoring and Assessment, 2020, 192(2), doi: 10.1007/s10661-019-7945-7.
[33] Wang X, Yan C X, Nie M H, et al. Physicochemical characteristics of UV-aged microplastic-derived DOM and its complexation mechanisms with sulfadiazine and copper [J]. Environmental Science, 2023, 44(11): 6159-6171.
[34] Liu Z H, Zhang Y Y, Xia F, et al. Effects of rainstorm events on water quality and spectral characteristics of dissolved organic matter in Qiandao Lake [J]. Acta Scientiae Circumstantiae, 2025, 45(10): 298-309.
[35] Cao M X, Ma H, Ye Y X, et al. Wildfire-derived pyrogenic dissolved organic matter (pyDOM) enhances riverine DOM reactivities and nitrogen metabolisms [J]. Environmental Science & Technology, 2025, 59(23), 11597-11606.
[36] Wang Q, Lechtenfeld O J, Rietveld, L C, et al. How aromatic dissolved organic matter differs in competitiveness against organic micropollutant adsorption [J]. Environmental Science and Ecotechnology, 2024, 21, doi: 10.1016/j.ese.2024.100392.
[37] Zhang Q R, Lv J T, He A, et al. Investigation with ESI FT-ICR MS on sorbent selectivity and comprehensive molecular composition of landfill leachate dissolved organic matter [J]. Water Research, 2023, 243, doi: 10.1016/j.watres.2023.120359.
[38] Zhou L L, Wang R G, Liu Y, et al. Plasma-induced conversion of polystyrene nanoplastics in water: Intermediates release, toxicity, and disinfection byproducts formation [J]. Chemical Engineering Journal, 2022, 433, doi: 10.1016/j.cej.2022.134543.
[39] Guo Z Y, Chen J W, Zhang S Y, et al. Influence of dissolved organic matter in natural water on photochemical transformation of organic micropollutants [J]. Chinese Science Bulletin, 2020, 65(26): 2786-2803.
[40] Wang K, Xu S J, Wang J J, et al. Insights into the photosensitivity and photobleaching of dissolved organic matter from microplastics: Structure-activity relationship and transformation mechanism [J]. Journal of Hazardous Materials, 2024, 480, doi: 10.1016/j.jhazmat.2024.135931.
[41] Carstea E M, Bridgeman J, Baker A, et al. Fluorescence spectroscopy for wastewater monitoring: A review [J]. Water Research, 2016, 95: 205-219.
[42] Zhu Y C, Jin Y, Liu X S, et al. Insight into interactions of heavy metals with livestock manure compost-derived dissolved organic matter using EEM-PARAFAC and 2D-FTIR-COS analyses [J]. Journal of Hazardous Materials,

2021, 420, doi: 10.1016/j.jhazmat.2021.126532.

[43] Ding L, Zhang H W, Chen H, et al. Photochemical transformation of microplastics-derived dissolved organic matter altered the photoaging of microplastics [J]. Journal of Hazardous Materials, 2025, 500, doi: 10.1016/j.jhazmat.2025.140477.

[44] Wang K, Ma S L, Li Z H, et al. New insights into the long-term leaching process of dissolved organic matter from microplastics: dynamic formation and transformation mechanism [J]. Environmental Science & Technology, 2025, doi: 10.1021/acs.est.5c07996.

[45] Lei X, Lei Y, Guan, J M, et al. Kinetics and transformations of diverse dissolved organic matter fractions with sulfate radicals [J]. Environmental Science & Technology, 2022, 56: 4457-4466.